Optical Materials 35 (2013) 868–874

Contents lists available at SciVerse ScienceDirect

Optical Materials

journal homepage: www.elsevier.com/locate/optmat

Ce-doped $Li_6Ln(BO_3)_3$ (Ln = Y, Gd) Single crystals fibers grown by micro-pulling down method and luminescence properties

T.S. Koroleva [a,b], M.M. Kidibaev [a], A. Nehari [b], C. Pedrini [b], K. Lebbou [b,*], A.N. Belsky [b], A.N. Tcherepanov [b,c], A.V. Ishchenko [b,c], V.Yu. Ivanov [c], I.N. Sedunova [c], O.S. Teslenko [c], L.V. Viktorov [c], B.V. Shulgin [c], L.H. Zheng [d], J. Xu [d], V. Kononets [b,e], O. Sidletskiy [e]

[a] Institute of Physical & Technical Problems and Materials Science of the National Academy of Sciences of the Kyrgyz Republic, 265-a, Prospect Chui, Bishkek 720071, Kyrgyzstan
[b] Laboratoire de Physico-Chimie des Matériaux Luminescents, Université de Lyon, Université Lyon 1, CNRS UMR5620, 69622 Villeurbanne Cedex, France
[c] Ural State Technical University – UPI named after the first President of Russia B.N. Yeltsin, Mira str., 19, Yekaterinburg 620002, Russia
[d] Shanghai Institute of Ceramics, Chinese Academy of Sciences, No. 588 Heshuo Road, Shanghai 201899, China
[e] Institute for Scintillation Material NAS of Ukraine, 60 Lenin Ave., 61001 Kharkiv, Ukraine

ARTICLE INFO

Article history:
Received 26 July 2012
Received in revised form 23 October 2012
Accepted 25 October 2012
Available online 12 December 2012

Keywords:
Crystal growth
Optical materials and properties
Scintillation
Ce^{3+}-doped LGBO
Ce^{3+}-doped LYBO

ABSTRACT

Ce^{3+}-doped borate crystal fibers of $Li_6Gd(BO_3)_3$ (LGBO) and $Li_6Y(BO_3)_3$ (LYBO) compositions are grown by the micro-pulling down (μ-PD) method for potential application in developing new neutron detectors. The ternary equilibrium diagram of Li_2O–Gd_2O_3–B_2O_3 is drawn and the preparations of homogeneous mixed LGBO and LYBO powders and growth conditions for single crystal fibers are discussed. Absorption, excitation and X-ray luminescence spectra are investigated. Absolute light yield derived from energy spectra and kinetic decay curves measured under α- and γ-scintillations of Ce^{3+}-doped LGBO and LYBO single crystal fibers is provided.

1. Introduction

Ce^{3+}-doped borates $Li_6Gd(BO_3)_3$ (LGBO) and $Li_6Y(BO_3)_3$ (LYBO) crystals are efficient scintillator materials [1–4]. Because they contain ^6Li and ^{10}B isotopes, they are attractive for neutron detection. The presence of ^{155}Gd, ^{157}Gd isotopes ray with MeV energy in LGBO crystals allows large capture cross-sections for thermal neutron detection. The knowledge of these materials family allows the potentiality of the fabrication of scintillating components using these crystals as active elements. Knitel et al. [5] firstly reported the scintillation properties of Ce^{3+}-doped LGBO and LYBO powder materials by X-ray excitation measurement. Czirr et al. [6] studied the characteristics of Ce^{3+}-doped LGBO crystal by thermal neutron excitation ((n,α) reaction with ^6Li, ^{10}B) and stimulated the (n,γ) nuclear reaction with odd isotopes of gadolinium. The LYBO system was investigated by Sablayrolles et al. and the crystals were grown by the Czochralski technique [4,7,8].

Van Eijk et al. [9,10] has suggested that LGBO crystals will have a high light yield (about 15,000 photons/MeV) and short decay times ($\tau \approx 27$ ns). As ^6Li, ^{10}B, ^{157}Gd, ^{155}Gd isotopes can react with the neutrons and then produce charged particles γ rays with MeV energy, which can excite some luminescence centers in the crystals and emit signals to be detected by the optical sensors [11], the crystals must be of good macroscopic and microscopic quality, they must be of high transparency far in the ultraviolet (UV) and have a good chemical stability and high reproducibility.

The advantage in substituting $Y^{3+}$and Gd^{3+} by Ce^{3+} in LYBO and LGBO crystals for neutrons below 150 MeV was shown in Ref. [12]. This advantage is related to the efficiency of (n,γ) reaction with odd isotopes of Gd begin to be worse than the efficiency of (n,α) reaction with ^6Li, ^{10}B. As LYBO crystals have lower effective atomic number ($Z_{eff} = 26$) than LGBO ($Z_{eff} = 46$), LYBO crystals are less sensitive to γ-radiation and can be recommended for neutron registration in γ-fields. Single crystal fibers could be of great interest to develop new neutron detector design. Growing high quality LGBO and LYBO-doped Ce^{3+} single crystal fibers could be a good way for the development of performed applications in specific scintillation detectors such neutron registration [13], scintillating fiber camera for space dosimetry [14], scintillation detector for electron- and beta-radiation [15].

In the frame of international collaboration, we have studied both the equilibrium diagram of LGBO system, the crystal growth of Ce^{3+}-doped LGBO and LYBO fibers by the micro-pulling down (μ-PD) technique and the scintillation properties.

* Corresponding author.
E-mail address: kheirreddine.lebbou@univ-lyon1.fr (K. Lebbou).

0925-3467/$ - see front matter © 2012 Elsevier B.V. All rights reserved.
http://dx.doi.org/10.1016/j.optmat.2012.10.045

2. Experimental part

2.1. Powders single phase preparation

The samples were prepared by solid state reaction from mixtures of Li_2CO_3, B_2O_3, Ln_2O_3 (Ln = Gd, Y) and CeO_2 powders (99.99% purity) cold pressed under 1 kgf cm^{-2} into discs of 15 mm diameter which were placed into an alumina crucible. They were weighed in proportions according to the following chemical reaction:

$$3Li_2CO_3 + \frac{3}{2}B_2O_3 + \frac{(1-x)}{2}Ln_2O_3 + x\cdot CeO_2 \xrightarrow{T} Li_6Ln_{1-x}Ce_xB_3O_9 + 3CO_2\uparrow$$

The mixed powders were pre-heated at 500 °C for 10 h to initiate the reaction and decompose carbonate. The second step is a sintering at 725 °C for 10 h in a flow of mixture of Ar/H_2 gas (95%/5%). After cooling to room temperature, the pellets were crushed and pressed again and then heated at 750 °C for 12 h. The same treatment was repeated several times in order to get a good homogeneity. In all cases, the phases were characterized by room temperature X-ray powder diffraction analysis using Cu Kα radiation. Fig. 1 shows room temperature X-ray powders diffraction of 1% Ce^{3+}-doped LGBO and LYBO single phase elaborated by solid state reaction.

2.2. Fibers single crystal grown from LGBO and LYBO congruently melting system

The fibers were grown from the melt by the micro-pulling down (μ-PD) technique [16–19]. The melt was contained in a crucible made of Pt plate of 0.1 mm thickness and Pt tube of 0.4–0.8 mm outer diameter and 0.02–0.06 mm wall thickness. The crystal fibers were grown with pulling rates between 0.02 and 0.1 mm/min using ⟨0 1 0⟩ LGBO seed. The length of the molten zone resulting in the most stable stationary growth conditions was maintained at about 0.05–0.1 mm. During LGBO and LYBO fiber crystal growth, increasing the length of the molten zone can be achieved by overheating of the melt that was often accompanied by Li_2O and B_2O_3 loses causing a change of the composition in the Li_2O–(Gd_2O_3/Y_2O_3)–B_2O_3 ternary equilibrium diagram.

2.3. Optical measurements

Absorption spectra were measured using a Perkin Elmer Lamda 900 spectrophotometer operating in the range 185–3300 nm. The X-ray luminescence, photoluminescence and photoexcitation spectra were recorded at room temperature using a Triax 320 monochromator equipped with a CCD camera cooled around 250 K by Pelletier effect, and EMI 9789 photomultiplier. The light excitation source was either a 500 W Xenon lamp and a Gemini 180 double monochromator. The measurements under X-ray excitation were performed using the X-ray source XRG3000 INEL operating at 35 kV with tungsten anode.

The *ALY* calculation was carried out under α-participle (radionuclide 239Pu) and γ-rays (241Am and 137Cs) sources using the single-electron pulse amplitude of photomultiplier (FEU-130) as a reference at weak illumination source in good agreement with the technique described in Ref. [20]. Because of the small size of the fibers, we have used α-participle (radionuclide 239Pu) source instead of neutron source. It is known that the mean free path of α-particles in matter is much smaller than absorption mean free path for neutrons.

Stilbene (1,2-diphenylethylene) and Tl:CsI scintillators were chosen as standard samples. The stilbene sample has constant characteristics, small decay time (less than 5 ns) and can be used to estimate the instrumental response of the measuring set-up. The Tl:CsI crystal is a well-known technical inorganic scintillator [21]. Light yield of stilbene crystals was determined by the compton edge at half-amplitude γ-spectrum [20]. The standard samples for measuring *ALY* were (a) technical detector (hermetic and packed with MgO reflector) stilbene-based 10 × 10 mm; (b) stilbene crystal 9 × 3 mm, packed with fluoroplastic ×reflector; (c) single crystal Tl:CsI 10 × 1.5 mm with fluoroplastic reflector. Blackened disc reflector with 1 mm centered hole was used for *ALY* measurement of Tl:CsI and 1% Ce^{3+}-doped LYBO crystals under α-excitation. Blackened disc is necessary to simplify the account of light collection ($K = 0.45 \pm 0.03$ in such geometry). The measurements of pulse–height spectra were performed using spectrometric amplifier and the ADC board production by SPC "Aspect".

Scintillation decay curves under α-and γ-sources were obtained using an oscilloscope Tektronix TDS5034B measuring the signal at the anode of the PMT. The studied crystal was placed in the PMT photocathode and the radioactive source was placed at distance less than 2 mm above the crystal. Optically transparent vaseline was used as immersion liquid.

3. Results and discussion

3.1. Ternary Li_2O–Gd_2O_3–B_2O_3 equilibrium diagram

Fig. 2 shows the drawn ternary equilibrium diagram from the experimental data. It describes the equilibrium between Gd_2O_3,

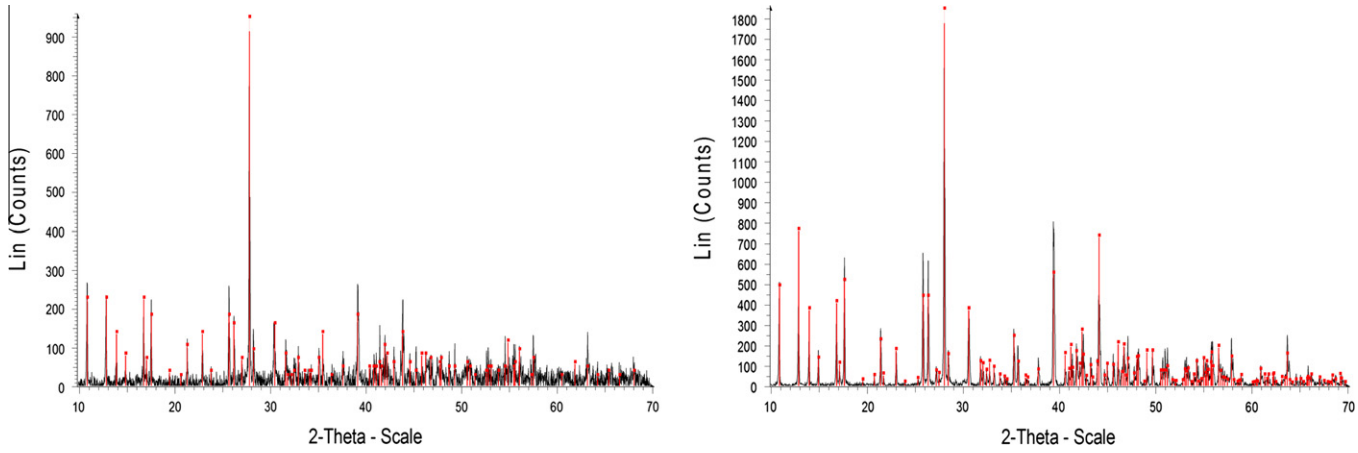

Fig. 1. Room temperature XRD diagrams of LGBO (left) and LYBO (right) powders doped with 1% Ce^{3+}.

B_2O_3 and Li_2O oxides. We confirm the presence of two ternary phases $LiGd_6O_5(BO_3)_3$ and $Li_6Gd(BO_3)_3$ [22]. The equilibrium phase diagram contains 13 three phases domains (Fig. 2) different than that proposed by Zhang et al. [22] which contains 14 three phases regions. We did not observe any metastable phase. This Li_2O–Gd_2O_3–B_2O_3 ternary system has been reinvestigated in order to define the phases involved during the crystal growth of LGBO. The results are coherent with the phase relationships proposed in Fig. 2. The solid phases mentioned in the literature are confirmed but the observed 13 three phases equilibria are not same. We noted the importance of the utilization of an excess of Li_2O (3%) and B_2O_3 (5%) to compensate the losses during solid state reaction.

3.2. Fibers single crystal grown from un-doped and Ce^{3+}-doped LGBO and LYBO systems

During growing single crystal fibers from congruently no wetting melt, it is not difficult to control the diameter of the fibers. Setting constant growth conditions (melt temperature, pulling rate, and sufficient length of meniscus that determines heat transfer from solid/liquid interface) allow the stationary stable sate. The growth of LGBO and LYBO single crystal fibers from stoichiometric melt is slightly difficult. Evaporation of Li_2O and B_2O_3 occurs and it is difficult to avoid the losses of these oxides. To minimize the losses of B_2O_3 and Li_2O oxides, the fibers were grown in atmosphere of air or argon containing 1% of oxygen. LGBO melts congruently at 850 ± 5 °C and LYBO at 865 ± 5 °C [23]. Unfortunately, the growth of single crystal fiber from an overheating melt from a stoichiometric mixture resulted in the continuous evaporation of Li_2O and B_2O_3 oxides corresponding to the enrichment of the melt with Gd_2O_3 (case of LGBO melt) and Y_2O_3 (case of LYBO melt) causing fast melt supercooling. The ⟨0 1 0⟩ LGBO seed crystal is dipped in the melt at the bottom of the crucible in the capillary die and the melt temperature is adjusted until a meniscus is supported. The molten zone and meniscus length are controlled by careful adjustment of the heater power. Both LGBO and LYBO melts have high viscosity which is comfortable to control the crystallization interface and overcome its inversion [24]. The dimension of the growth zone, including the meniscus height and the fiber diameter, were measured directly from the screen of the monitor during the growth process.

Temperature of the melt inside the crucible is an important data, because it is directly connected to the driving force of the melt flow. To control the growth process, we have followed melt temperature by an optical pyrometer (±2 °C). The evaporation of Li_2O and B_2O_3 caused a strong instability of the surface tensions because of Marangoni flows and the melt boiling. The crystals were grown at low pulling rate belonging to the range [0.02–0.1 mm/min] and were 800 μm in diameter, close to the diameter of the crucible capillary die. They were transparent, colorless and smooth surface. The typical length of the molten zone corresponding to the stationary state was about 50 μm and the crystallization interface was flat and stable. The length of the fiber was up to 30 mm depending on the starting raw material, and 100% of the liquid was crystallized into the fibers. Whatever the starting composition prepared in this work ($Ce^{3+} \leqslant$ 1at%), we had not seen strong spiral growth as observed in Czochralski LGBO crystal growth [3]. During stationary stable growth, disconnection of the fiber from the molten zone was not observed. Fig. 3 shows the un-doped and Ce^{3+}-doped LGBO and LYBO grown fibers under stationary stable regime corresponding to flat interface. The diameter is stable with high reproducibility, the grown LGBO and LYBO fibers were slightly faceted and were free from scattering and core region. The substitution of gadolinium (Gd^{3+}) and yttrium (Y^{3+}) by cerium (Ce^{3+}) does not affect the symmetry and the crystallography of the crystals. We have checked this result by room temperature X-ray diffraction. Neither impurities nor secondary phases have been observed. The LGBO and LYBO systems consist of boron triangularly coordinated to oxygen atoms. The lithium atoms occupy six independent positions and are surrounded by four or five oxygen atoms. The symmetry of both Y^{3+} and Gd^{3+} ion sites is C1 (distorted cube) [8–25]. Both LGBO and LYBO crystallizes in the monoclinic system with the space group $P2_1/c$ with the refined parameters measured on the fibers single crystals grown by micro-pulling down technique as can seen in Table 1.

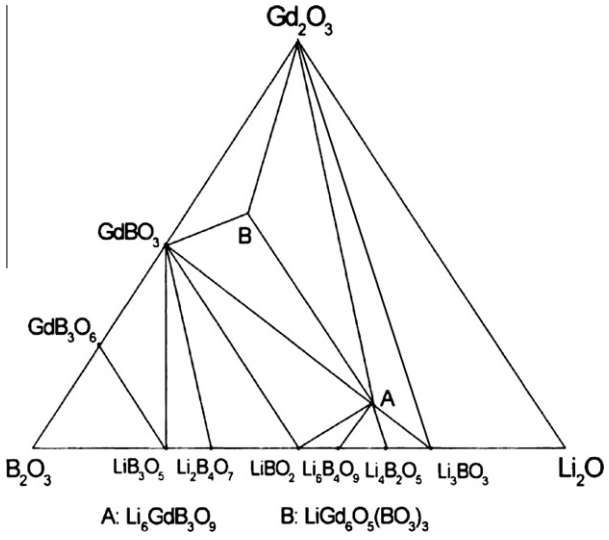

Fig. 2. Phase equilibrium diagram for the ternary system Li_2O–Gd_2O_3–B_2O_3 at 750 °C and PO_2 = 1 bar.

3.3. Luminescence properties

Fig. 4 shows room temperature absorption, photoexcitation and photoluminescence spectra of Ce-doped LYBO and LGBO single crystals fibers. The absorption spectra of Ce^{3+}-doped LYBO crystal (Fig. 4a) is characterized by a wide nonstructural band with flat, non-transparent part at 200–325 nm. Such absorption spectra are not typical of Ce^{3+} contained borates. The right edge of the Ce^{3+}-doped LYBO and the CeO_2 oxide [26] absorption spectra are similar. Because of the growth atmosphere (air and argon containing 1% oxygen), the Ce^{3+}-doped LYBO fibers contain high amount of Ce^{4+} ions. The absorption spectra of Ce-doped LGBO fiber is shown in Fig. 5a. It is characterized by several absorption broad bands of Ce^{4+} ion at 203 nm, 216 nm, 240 nm (probably $O^{2-} \rightarrow Ce^{4+}$ charge transfer bands) [27], Ce^{3+} ion at 307 nm and 346 nm (4f → 5d bands) [27] and several narrow Gd^{3+} 4f lines near 274 nm ($^8S_{\frac{7}{2}} \rightarrow {}^6I_j$ transitions). The excitation luminescence spectra of Ce^{3+}-doped LGBO and LYBO crystals are similar (Figs. 4b and 5b). In the case of Ce^{3+}-doped LYBO, three 4f–5d bands at 255 nm, 310 nm and 350 nm were observed. The 5d–4f spectrum of Ce^{3+}-doped LGBO crystal is characterized by a broad asymmetrical band at 255 nm and a series of several weakly resolved broad bands in the range of 280–380 nm. From 200 nm to 400 nm, the measured excitation spectra are similar to Ce^{3+}-doped fluoro-apatites [28], and can be attributed to 4f–5d transitions in Ce^{3+} ions [28]. In addition, we register the presence of Gd^{3+} band at 274 nm, which may indicate the possibility of $Gd^{3+} \rightarrow Ce^{3+}$ energy transfer.

The photoluminescence and X-ray luminescence spectra of 1% Ce-doped LYBO and LGBO crystals have similar characteristics (Figs. 4c, 5c and 6). They have multiple profile and locates at 360–500 nm with maximum at 405 nm and FWHM 61 nm. The luminescence is attributed to the electronic d–f transitions in Ce^{3+} ion ($^2D_{\frac{3}{2}} \rightarrow {}^2F_{\frac{7}{2}}$ and $^2D_{\frac{3}{2}} \rightarrow {}^2F_{\frac{5}{2}}$) [28].

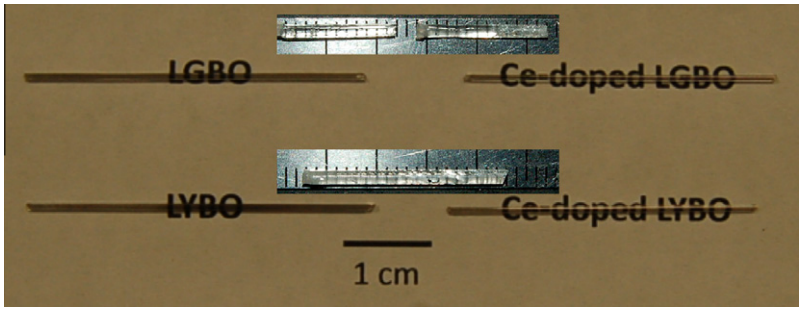

Fig. 3. Photograph of the as grown un-doped and Ce^{3+}-doped LGBO and LYBO Crystals.

Table 1
Crystallographic parameters measured on the different fibers grown by μ-PD.

	Space group	*a* (Å)	*b* (Å)	*c* (Å)	*β*°	*Z*	*ρ*
$Li_6Gd(BO_3)_3$	$P2_1/c$	7.2198(3)	16.5112(5)	6.7044(7)	105.3642(2)	4	3.239(4)
$Li_6Y(BO_3)_3$	$P2_1/c$	7.1498(6)	16.3698(4)	6.6195(6)	105.3311(3)	4	2.758(5)
$Li_6Gd_{0.99}Ce_{0.01}(BO_3)_3$	$P2_1/c$	7.2201(5)	16.5202(5)	6.7042(4)	105.3812(3)	4	3.158(7)
$Li_6Y_{0.99}Ce_{0.01}(BO_3)_3$	$P2_1/c$	7.1487(5)	16.3612(3)	6.6135(7)	105.3303(8)	4	2.615(3)

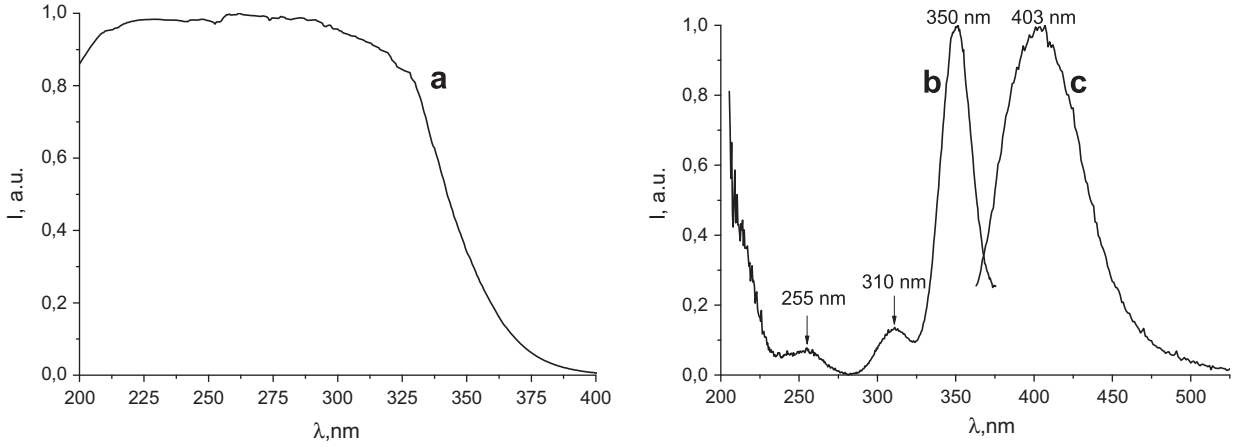

Fig. 4. The absorption spectra (a), excitation spectra (b) of the band at 400 nm and photoluminescence spectra (c) excitation at 310 nm of 1% Ce^{3+}-doped LYBO as-grown fiber crystal.

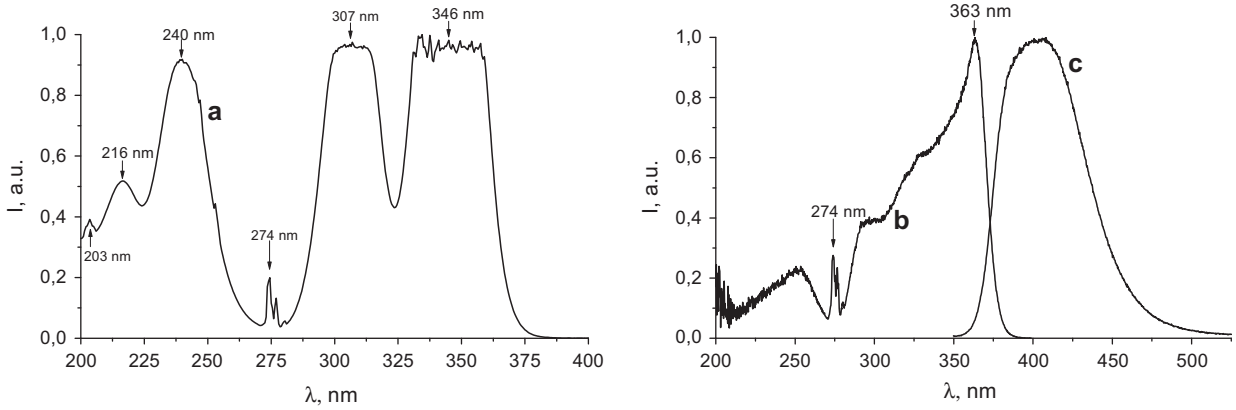

Fig. 5. The absorption spectra (a), excitation spectra (b) of the band at 400 nm and photoluminescence spectra (c) excited at 310 nm of 1% Ce^{3+}-doped LGBO as-grown fiber crystal.

3.4. Scintillation properties. Absolute light yield and kinetic properties

The absolute light yield (*ALY*) of α- and γ-scintillations of Ce-doped LYBO and LGBO fibers were measured under ^{239}Pu and ^{241}Am excitation.

Fig. 7 shows the pulse-height spectra of the 1% Ce-doped LYBO. Only one photopeak in α-scintillation spectra (Fig. 7a) with maximum at 5.15 MeV (the energy of α particles of ^{239}Pu) was observed. For γ-scintillations, two photopeaks (Fig. 7b) with maximum at 26.3 and 59.5 keV (γ-ray lines of ^{241}Am isotope) were observed.

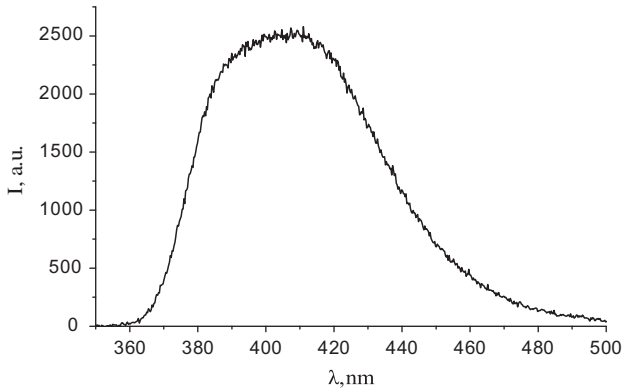

Fig. 6. The XRL spectrum of 1% Ce^{3+}-doped LYBO fiber crystal.

In the case of Ce-doped LGBO fiber, the energy spectra have been measured only under ^{239}Pu excitation. Under γ-sources, we did not detect any photopeaks, but a significant increase in counting rate have been observed. Fig. 8 shows the pulse-heights spectra of 0.8% and 1% Ce-doped LGBO under α particles excitation. The absence of photopeak in the energy spectrum under γ-source can be attributed to the low optical quality of the grown fiber. The LYBO:Ce crystal fibers was the best quality.

Table 2 shows the obtained results from the energy spectra used to calculate *ALY*. The calculating accuracy is about 25%. It is caused by appreciable error of working out of light collection K_{lc} [20]. In addition, in Table 2 we have presented *ALY* values of CsI–Tl and stilbene scintillators. They are in good agreement with the known data in [21,29].

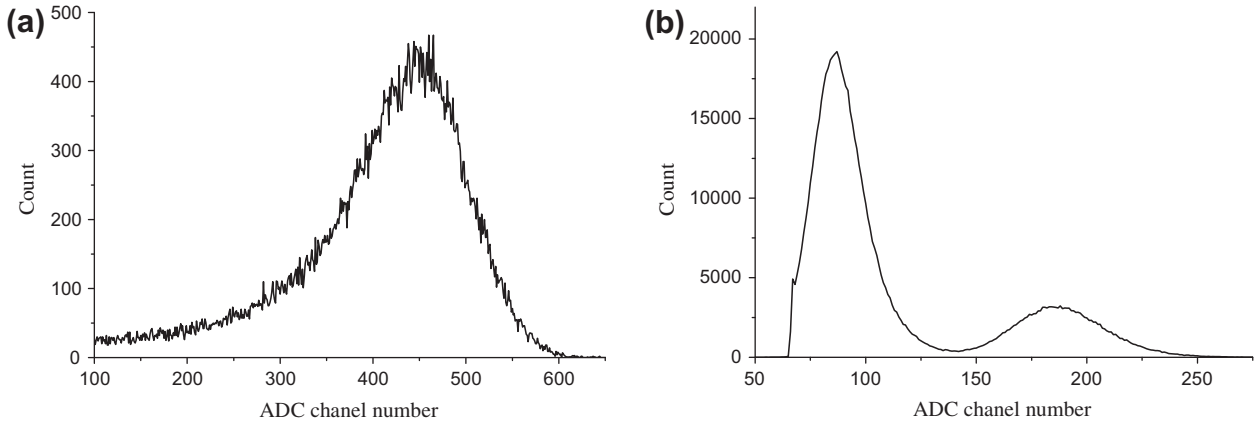

Fig. 7. Pulse-height spectra of α- (a) and γ-scintillations (b) of 1% Ce^{3+}-doped LYBO fiber crystal under excitation by ^{239}Pu и ^{241}Am radiation source.

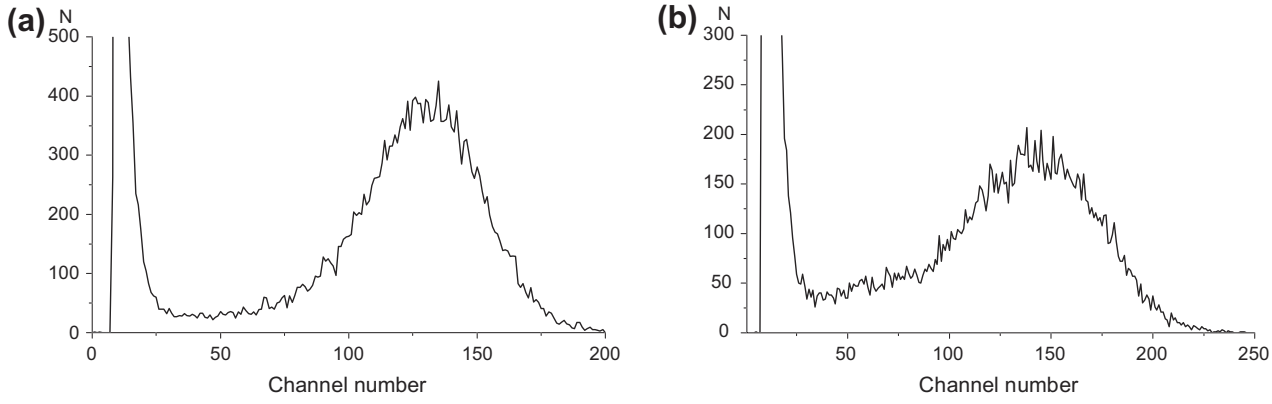

Fig. 8. Energy spectra of ^{239}Pu measured on Ce^{3+}-doped LGBO fiber crystals (a) Ce = 1% (b) Ce = 0.8% concentration.

Table 2
Results of *ALY* calculating.

Specimens	A_{sc}/A_o a.u.	E_{exc} keV	K_{sm}	K_{il}	K_{lc}	*ALY* photon/keV	*ALY*[a] photon/keV
γ-Scintillations							
LYBO:1% Ce	129	59.5	0.968	0.81	0.60	19.0	1.2 [5]
LGBO:1% Ce	93.1	59.5	0.966	0.82	0.60	13.6	17 [9]
CsI–Tl	126	59.5	0.4	0.7	0.72	63.2	61.0 [20,21]
Stilbene	900	662.7	1.0	1.0	0.70	8.0	11.4 [29]
α-Scintillations							
LYBO:1% Ce	3030	5150	0.968	0.85	0.60	4.9	–
LGBO:1% Ce	2723.3	5150	0.966	0.90	0.60	4.2	
CsI–Tl	8200	5150	0.4	0.8	0.45	43.6	–
Stilbene	760	5150	1.0	1.0	0.70	0.87	–

[a] A_{sc}/A_o – amplitude of scintillations to amplitude of one-electron peak ratio; E_{exc} – energy of excitation particles, keV; K_{sm} – spectral matching factor [9]; K_{il} – inertial losses factor; K_{lc} – light collection factor.

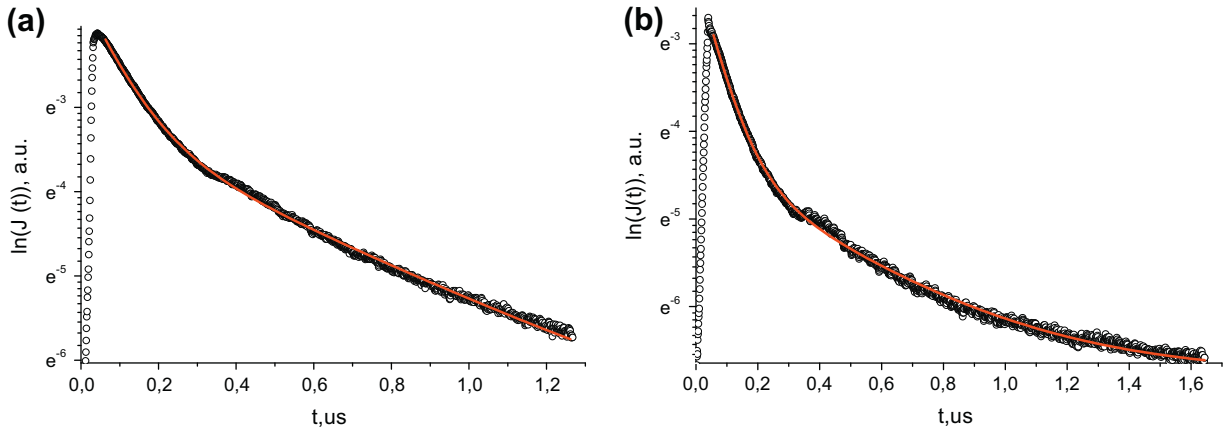

Fig. 9. Decay curves $J(t)$ of scintillations of 1% Ce^{3+}-doped LGBO crystal under α-particles (a) and γ-ray (b) excitation.

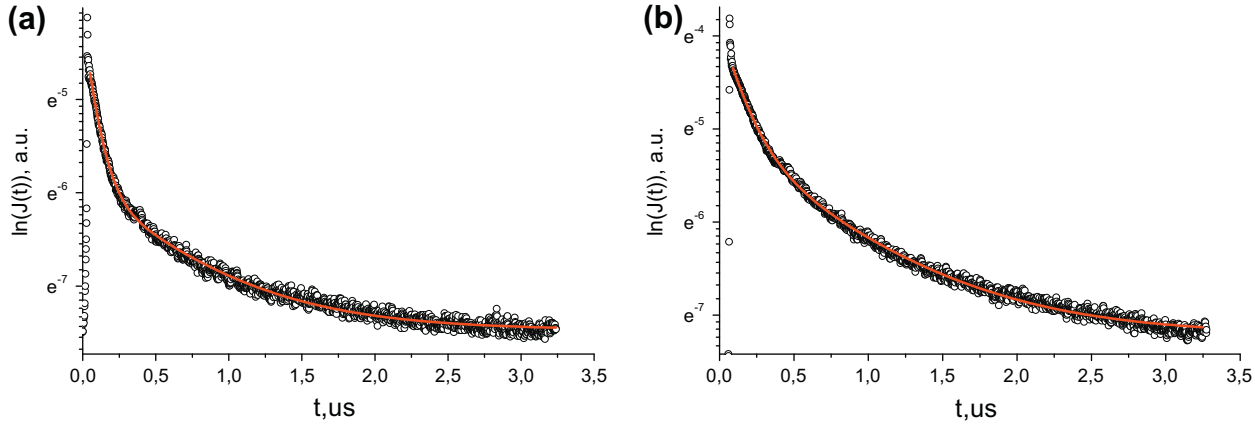

Fig. 10. Decay curves $J(t)$ of scintillations of 1% Ce^{3+}-doped LGBO crystal under α-particles (a) and γ-ray (b) excitation.

Table 3
The kinetic properties of LYBO:1% Ce, LGBO:1% Ce and stilbene.

Specimen	Excitation type	τ_1, ns	τ_2, ns	Initial amplitudes ratio J_1/J_2
1% Ce^{3+}-doped LYBO	α (^{239}Pu)	87	456	2.1
	γ (^{137}Cs)	66	397	4.0
1% Ce^{3+}-doped LGBO	α (^{239}Pu)	14	721	1.8
	γ (^{137}Cs)	75	635	3.6
Stilbene	α (^{239}Pu)	6	658	13.4
	γ (^{137}Cs)	6	175	1.3

For both Ce-doped LYBO and LGBO fibers, the measured *ALY* values under α-source were almost equal. However, by taking in consideration that the effective atomic number of LGBO:Ce (Z_{eff} = 46) is almost two times higher than LYBO:Ce (Z_{eff} = 26), we believe that the efficiency detection of neutrons for LYBO:Ce will be higher than LGBO:Ce.

The value of *ALY* under γ-source for both compositions were also approximately equal. The significant difference in light output under γ-source has been obtained in Ref. [5]. However, in contrast to [5], the obtained light yield of LYBO:Ce for γ-scintillation is 10 times higher.

3.5. Kinetic properties

The decay curve measurements were carried out using ^{239}Pu α-source with energy 5.15 MeV and ^{137}Cs γ-source with energy 662.7 keV. Figs. 9 and 10 show the decay curves of 1% Ce-doped LYBO: and 1% Ce-doped LGBO for α- and γ-scintillations.

The decay curves of 1% Ce-doped LYBO crystals are well approximated by two exponential curves. Table 3 lists the approximation parameters. The fast-slow components relation depends significantly on the type of excitation: in case of α-excitation relation of initial amplitudes J_1/J_2 is 2.1 for LYBO and 1.8 for LGBO, in case of γ-excitation it is 4.0 for LYBO and 3.6 for LGBO. Due to difference in the form of the pulses using software and hardware methods, α-scintillation can be discriminated on the γ-scintillation background, as well as in the case of stilbene for neutron on the γ-radiation background.

4. Conclusion

The ternary Li_2O–Gd_2O_3–B_2O_3 system has been investigated. The results are coherent with phase relationships proposed in Fig. 2. The solid phases mentioned in the literature are confirmed but the observed equilibrium domains are not identical. The substitution of Gd^{3+} and Y^{3+} by Ce^{3+} in LGBO and LYBO crystals do not change site symmetry. Acceptable quality of Ce^{3+}-doped LGBO and Ce^{3+}-doped LYBO fiber single crystals were successfully grown by the micro-pulling down technique. The melt behavior of the samples doped with low cerium concentration is close to the congruently melting point of LGBO and LYBO. But the B_2O_3 and Li_2O oxides are important to control the congruent melt behavior and to overcome the change of the composition in LGBO and LYBO equilibrium diagram during pulling the fibers.

Ce-doped LYBO and LGBO fibers crystals scintillation properties were carried out, absolute light yield of scintillations under α- and γ-excitation was measured; decay curves and main characteristics of photoexcitation, XRL spectrum of the crystals were described.

According to our results 1% Ce-doped $Li_6Y(BO_3)_3$ grown in argon atmosphere was the best fiber crystal. The *ALY* of 1% Ce-doped LYBO fiber crystal α-scintillations is 5.3 times higher than stilbene scintillator. Under the influence of α particles and γ radiation, the existence of differences in the decay time show that the detectors based on LYBO:Ce and LGBO:Ce fiber crystals can be used for separate detection of neutron in n-γ-fields.

References

[1] J.P. Chaminade, O. Viraphong, F. Guillen, C. Fouassier, B. Czin, Nuclear Sciences Symposium Conference, IEEE, vol. 1, 2000, p. 189.
[2] A.N. Shekhovtsov, A.V. Tolmachev, M.F. Dubovik, E.F. Dolzhenkova, T.I. Korshikova, B.V. Grinyov, V.N. Baumer, O.V. Zelenskaya, J. Cryst. Growth 242 (2002) 167.
[3] J.P. Chaminade, O. Viraphong, S. Miyazawa, J. Cryst. Growth 237–239 (2002) 864.
[4] E.F. Dolzhenkova, V.N. Baumer, A.V. Tolmachev, R.P. Yavetsky, Mater. Res. Bull. 41 (2006) 530.
[5] J.M. Knitel, P. Dorenbos, E.W.C. Van Eijk, B. Plasteig, B. Viana, A. Kahn-Harari, D. Vivien, Nucl. Instrum. Methods Phys. Res. A 443 (2000) 364.
[6] B.J. Czirr, M.G. MacGillivray, R.R. MacGillivray, J.P. Seddon, NIM A 424 (1999) 15.
[7] J. Sablayrolles, V. Jubera, F. Guillen, R. Decourt, M. Couzi, J.P. Chaminade, A. Garcia, Opt. Commun. 280 (2007) 103.
[8] A. Brenier, A. Yoshikawa, K. Lebbou, A. Jouini, O. Aloui-Lebbou, G. Boulon, T. Fukuda, J. Lumin. 126 (2007) 547.
[9] E.W.C. Van Eijk, New Scintillators, new light sensors, new applications, in: Proceedings of Inorganic Scintillators and their Applications, 1997, p. 5.
[10] E.W.C. Van Eijk, Radiat. Meas. 38 (2004) 337.
[11] J.M. Knitel, P. Dorenbos, E.W.C. Van Eijk, B. Plasteig, B. Viana, A. Kahn-Harari, D. Vivien, Nucl. Instrum. Methods Phys. Res. A 443 (2000) 364.
[12] J.B. Czirr, G.M. MacGillivray, R.R. MacGillivray, P.J. Seddon, Nucl. Instrum. Methods Phys. Res. A 424 (1999) 15.
[13] B.V. Shulgin, T.S. Koroleva, et al., in: Proceedings of the 8th International Conference on Inorganic Scintillators and their Use in Scientific and Industrial Applications, Alushta, Ukraine, 2005, p. 109.
[14] K. Terasawa, T. Doke, K. Hara, N. Hasebe, IEEE Trans. Nucl. Sci. 48 (2001) 1118.
[15] I.N. Sedunova, V.Yu. Ivanov, V.N. Churmanov, et al., Probl. Spectrosc. Spectrom. 26 (2010) 142. in Russian.
[16] K. Lebbou, A. Yoshikawa, T. Fukuda, M.Th. Cohen Adad, G. Boulon, Mat. Res. Bull. V8 (2000) 35.
[17] V. Chani, K. Lebbou, Cryst. Res. Technol. 41 (2006) 972.
[18] K. Lebbou, D. Perrodin, Adv. Mater. Res., in: T. Fukuda, V. Chani (Eds.), Shaped Crystal Growth by Micro-Pulling-Down Technique, Springer Verlag, Berlin, 2007, p. 173.
[19] A. Yoshikawa, M. Nikl, G. Boulon, T. Fukuda, Opt. Mater. 30 (2007) 6.
[20] L.V. Viktorov, A.P. Volkov, A.V. Kruzhalov, S.V. Podurovskiy, V.B. Shulgin, Atom. Energia 71 (1) (1991) 64. 1991. Num. 1. p. 64–67. (In Russian)..
[21] I. Holl, E. Lorenz, G. Mageras, A measurement of the light yield of common inorganic scintillators, IEEE Trans. Nucl. Sci. 35 (1988) 105.
[22] Y. Zhang, X.L. Chen, J.K. Liang, T. Xu, J. Alloys Compd. 348 (2003) 314.
[23] O.Aloui, Ph.D. thesis, Claude Bernard Lyon 1 University, November 26, 2002 (in French).
[24] F. Yang, S.K. Pan, D.Z. Ding, H. Ren, Cryst. Res. Technol. 44 (2009) 141.
[25] G.K. Abdullaev, K.S. Mamedov, P.F. Rza-Zade, S.A. Guseinnova, G.G. Dzadarov, Russ. J. Inorg. Chem. 22 (1977) 1765.
[26] A.A. Hosseini, C.A. Hogarth, J. Beynon, Optical absorption in CeO_2–V_2O_5 evaporate thin films, Sci. I. R. Iran 5 (1994) 135.
[27] A.M. Efimov, A.I. Ignat'ev, N.V. Nikonorov, E.S. Postnikov, Opt. Spectrosc. 111 (3) (2011) 426.
[28] Q. Zeng, H. Liang, G. Zhang, MD. Birowosuto, Z. Tian, H. Lin, Y. Fu, P. Dorenbos, Q. Su, J. Phys.: Condens. Matter 18 (2006) 9549.
[29] S.K. Lee, B.H. Kang, W.G. Lee, J.K. Kim, Y.K. Kim, N.Z. Galunov, G.D. Kim, Scintillation properties of Large Area Composite Stilbene Scintillator For Neutron Detection, in: IEEE Nuclear Science Symposium Conference Record, 2009, p. 1509.